Journal of Power Sources 259 (2014) 227–232

Contents lists available at ScienceDirect

Journal of Power Sources

journal homepage: www.elsevier.com/locate/jpowsour

A facile hydrothermal route to iron(III) oxide with conductive additives as composite anode for lithium ion batteries

Gen Chen [a], Rodrigo Rodriguez [a], Ling Fei [a], Yun Xu [a], Shuguang Deng [a], Sergei Smirnov [b], Hongmei Luo [a,*]

[a] Department of Chemical Engineering, New Mexico State University, Las Cruces, NM 88003, United States
[b] Department of Chemistry and Biochemistry, New Mexico State University, Las Cruces, NM 88003, United States

HIGHLIGHTS

- Fe_2O_3 nanoparticles can be prepared *via* a facile hydrothermal route.
- Reduced graphite oxide and polymer have been introduced for composite materials.
- The conductive additives can enhance the electrochemical performances.
- Conductive additives may work in different way to improve the electrochemical performances.

GRAPHICAL ABSTRACT

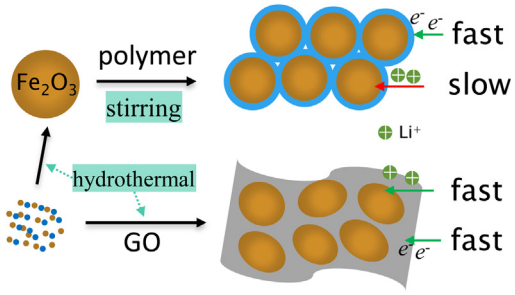

ARTICLE INFO

Article history:
Received 15 November 2013
Received in revised form
22 February 2014
Accepted 25 February 2014
Available online 7 March 2014

Keywords:
Iron oxide
Reduced graphite oxide
Conductive polymer
Hydrothermal
Lithium ion battery

ABSTRACT

We report a facile hydrothermal route for the synthesis of Fe_2O_3 nanoparticles and their composites with conductive additives, reduced graphite oxide (rGO) and conductive polymer PEDOT:PSS, as anode materials for lithium ion batteries (LIBs). The addition of conductive polymer layer on Fe_2O_3 nanoparticles may facilitate the electron transport but hinders the Li^+ ion insertion at higher current density. On the other hand, Fe_2O_3@rGO prepared by growing Fe_2O_3 nanoparticles directly on rGO sheets shows the best electrochemical behavior due to a beneficial combination of the rGO nanosheets partially wrapped around Fe_2O_3 which facilitates both the electron transport and the Li^+ ion insertion. The enhanced conductivity of the composites was proved. The high specific capacity and stable rate performance of Fe_2O_3@rGO composites encourages their further study to be potential candidate for the anode materials in LIBs. These results will be helpful in further elucidation of the role of conductive additives in improving the electrochemical performance of Fe_2O_3 based composite anodes and this simple synthetic strategy can be applied for the large scale production of metal oxides with conductive additives for LIBs.

1. Introduction

Rechargeable lithium-ion batteries (LIBs) currently provide the dominant power source for a range of devices including portable electronic devices and electric vehicles due to their high energy and power density. Novel LIBs are considered to be a promising option in the quest to alleviate problems associated with the rapid depletion of fossil fuels and deterioration of the global eco-environment. The interest in exploring new electrode materials for LIBs has been drastically increasing due to the surging demands for clean energy [1–3]. Currently, graphite-based anodes, which can only deliver a theoretical capacity of about 372 mA h g^{-1}, are

* Corresponding author. Tel.: +1 575 646 4204; fax: +1 575 646 7706.
E-mail addresses: hluo@nmsu.edu, luohongmeitulane@yahoo.com (H. Luo).

http://dx.doi.org/10.1016/j.jpowsour.2014.02.096
0378-7753/

applied in most commercial rechargeable LIBs. This type of batteries has a relatively low energy-storage ability and does not meet the demands for increasing energy density. Other alternatives, such as iron oxide (Fe_2O_3), have attracted increasing attention. Fe_2O_3 is a very promising candidate as anode material in rechargeable LIBs because it can store up to six Li per formula unit ($Fe_2O_3 + 6Li \leftrightarrow 3Li_2O + 2Fe$) *via* reversible reactions, resulting in a high theoretical capacity of 1007 mA h g^{-1}. Low cost, ease of fabrication and environmental friendliness are additional advantages that can accelerate the large scale commercial applications of Fe_2O_3 in energy storage. In spite of these excellent characteristics, Fe_2O_3 suffers from poor conductivity, large volume change and voltage hysteresis in the electrochemical reaction [4,5], which strongly limits its practical application. To overcome these disadvantages, the research has been focusing on the following aspects: (i) synthesis of nanosized Fe_2O_3 materials with large surface area, which can greatly enhance the contact area between the active material and electrolyte and shorten the diffusion path of lithium ions [6–8]; (ii) novel morphologies of the microstructures such as hollow spheres [6,9], nanorods [10], spindles [11], nanotubes [12], nanocubes [13] proposed as means of advancing superior electrochemical kinetics and remarkable structural stability; and (iii) composites of Fe_2O_3 with different carbon or polymer additives designed to improve the conductivity and the electrochemical performances [14–17].

In this work, a facile surfactant-free hydrothermal route was applied for the synthesis of Fe_2O_3 nanoparticles coated with conductive additives (reduced graphite oxide (rGO) or polymer) as the composite anode for LIBs. Improved conductivity and structural stability of such Fe_2O_3 composites demonstrate superior cycling and rate performances as compared to the bare Fe_2O_3 nanoparticles. The rGO nanosheets wrapped structure, Fe_2O_3@rGO, demonstrates better performance than the polymer coated one, which can be attributed to the faster lithium ion transport kinetics. Relatively good electrochemical performance of the composite anodes, such as large reversible capacity, high Coulombic efficiency, slow capacity fading, and stable rate capacity upon increased currents, indicates that this simple synthetic strategy could be further applied to the large scale production of metal oxides with conductive additives for LIBs.

2. Experimental section

2.1. Synthesis

All chemicals purchased from Sigma–Aldrich Co. LLC were of analytical grade and used as starting materials without further purification. Fe_2O_3 nanoparticles were synthesized by a hydrothermal method which is similar to a previous work [18] except for different ion precursor. In a typical procedure, 3 mL of triethylamine (Et_3N) was added to 1 mmol of $FeCl_3 \cdot 6H_2O$ dissolved in 25 mL of DI water under continuous stirring for 20 min. Thus formed suspension was transferred into a Teflon-lined stainless steel autoclave of 50 mL capacity and cooked at 160 °C for 18 h. The final product was washed with DI water and absolute ethanol several times then dried in vacuum oven at 60 °C for 6 h.

Graphite oxide (GO) was synthesized from natural graphite by a modified Hummers method [19] and the GO nanosheets were dispersed in DI water to achieve the concentration of ~6 mg mL^{-1}. Previous reports have already demonstrated that GO would be reduced in an aqueous solution under thermal treatment [20–23]. In our procedure, 5 mL of such GO dispersion was added to 28 mL of the described above suspension under continuous stirring and then similar hydrothermal treatment was applied to produce Fe_2O_3 directly on rGO nanosheets. Poly(3,4-ethylenedioxythiophene)-poly(styrenesulfonate) (PEDOT:PSS) in high-conductivity grade which could be originally dispersed in water enabled its *ex situ* coating by mechanical stirring and was used in preparing Fe_2O_3 composite with conductive polymer (labeled as Fe_2O_3@Polymer). Typically, 100 mg of as-prepared Fe_2O_3 powder was dispersed in DI water under ultrasonic treatment for 30 min and 5 mL of PEDOT:PSS polymer solution (~2.4% by weight in DI water) was added dropwise under continuous stirring for additional 30 min. The mixture was stirred for additional 24 h. Subsequently, Fe_2O_3@Polymer was collected by centrifuging at 2000 RPM for 5 min and dried in an oven at 60 °C for 6 h.

2.2. Characterization

The structure and crystallinity of the obtained products were determined using a Rigaku MiniFlex II X-ray powder diffractometer (XRD) with Cu Kα radiation ($\lambda = 1.5418$ Å). The size and morphology were determined by S-3400NII scanning electron microscopy (SEM), Hitachi H-7650 transmission electron microscope (TEM), JEOL-2010 high resolution transmission electron microscope (HRTEM). Thermal behavior of composites was characterized by PerkinElmer Pyris 1 thermogravimetric analysis (TGA) in the temperature range of 25–700 °C at a heating rate of 10 °C min^{-1} in air.

2.3. Electrochemical analyses

The electrochemical experiments were performed using 2032-type coin cells, which were assembled in an argon-filled dry glovebox (Vigor Gas Purification Technologies, Inc.) with the trace amounts of oxygen and moisture below 1 ppm. The working electrodes were prepared by casting the slurry (70 wt% of active material, 20 wt% of carbon black, and 10 wt% of polyacrylic acid binder) on nickel foam (MTI). The electrode loading amount was around 4.0 mg cm^{-2}. The counter electrode was made of lithium metal. The electrolyte was composed of 1 M $LiPF_6$ in a mixture of ethylene carbonate and dimethyl carbonate (1:1 by volume). The electrochemical performance was evaluated by galvanostatic charge/discharge cycling on an LAND CT2001A multi-channel battery testing system at room temperature in the voltage range between 0.01 and 3 V versus Li^+/Li. Specific capacity is calculated based on the mass of active material. Cyclic voltammetry (CV) curves of so prepared coin-cell samples were obtained on a VersaSTAT 4 with a scan rate of 0.2 mV s^{-1}. The electrochemical impedance spectra (EIS) of fresh samples were recorded on a CHI-680A (CH Instruments, Inc) electrochemical workstation using zero bias potential.

3. Results and discussion

Fig. 1 shows a typical XRD pattern of the as-synthesized Fe_2O_3 nanoparticles. All the diffraction peaks can be readily indexed as the rhombohedral Fe_2O_3 (JCPDS 33-0664) with the lattice constants $a = 5.036$ Å and $c = 13.749$ Å (space group: *R-3c* (No. 167)). No other peaks were observed, indicating a high purity of the final products obtained under current experimental conditions. Fig. 1B and C presents the low- and high-magnification TEM images of the as-prepared Fe_2O_3 nanoparticles, indicating that products with good uniformity can be obtained on a large scale. The size of Fe_2O_3 nanoparticles is in the range of 100–200 nm with the average size near 180 nm. A good homogeneity illustrated by SEM images in Fig. S1 (Supporting information). HRTEM and Fast Fourier Transform (FFT) images shown in Fig. 1D confirm that the Fe_2O_3 nanoparticles are structurally uniform and of good crystallinity. The distance between the adjacent planes, 0.272 nm, corresponds to (104) plane of the rhombohedral Fe_2O_3.

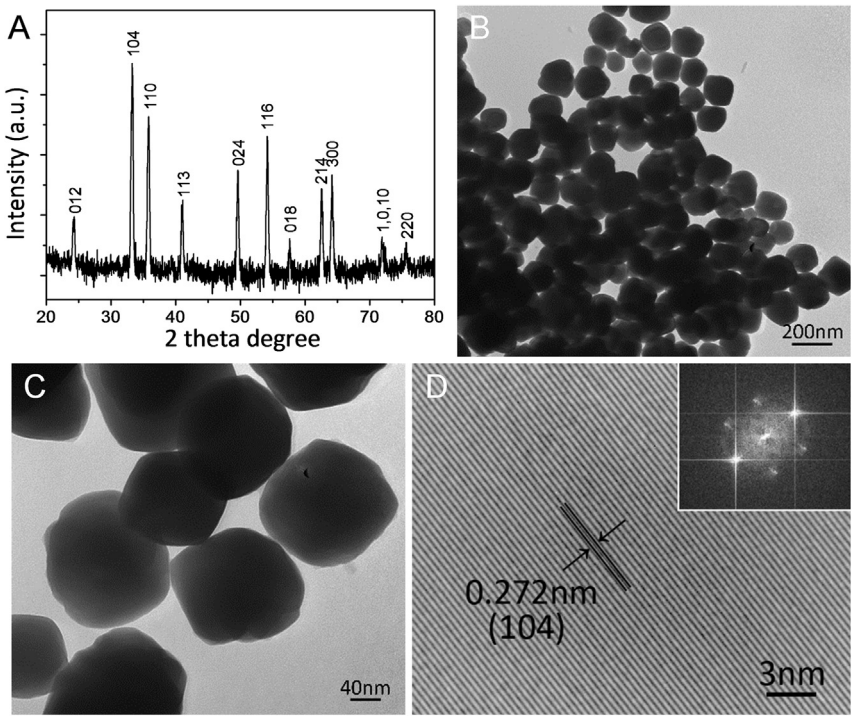

Fig. 1. (A) XRD pattern; (B) low-, (C) high-magnification TEM images of Fe_2O_3 nanoparticles; (D) HRTEM and FFT image (inset) of as-prepared Fe_2O_3 nanoparticles.

Scheme 1 illustrates the two routes used here for production of Fe_2O_3 composites with conductive additives. Based on the simple hydrothermal treatment, rGO nanosheets and conductive polymer PEDOT:PSS have been introduced *in situ* and *ex situ* for production of the composites, respectively. Inspired by the work of Han et al. on polypyrrole-coated Fe_2O_3@C [15], we introduced a different conductive polymer with a goal to facilitate formation of a stable solid electrolyte interface (SEI) layer and enhance electronic conductivity. We compared it with another common additive, rGO, which was shown before to improve the electrochemical performance of electrode materials [19,24,25]. Typical TEM images of the composite materials are displayed in Fig. 2. As seen in Fig. 2A, PEDOT:PSS coats Fe_2O_3 nanoparticles and works as conductive matrix supporting and connecting the nanoparticles. Their sizes remain the same as for the bare Fe_2O_3, indicating that mechanical stirring doesn't affect their structure and morphology. A close observation of such Fe_2O_3@Polymer clearly reveals the thin film on the surface of Fe_2O_3 nanoparticles and also clusters of the polymer (see Fig. 2B). The polymer clusters and gel-like thin coating in Fe_2O_3@Polymer are critical to the improved performance; they buffer mechanical strains in Fe_2O_3, prevent pollution by impurities, and bridge the Fe_2O_3@Polymer together to combine Fe_2O_3 into larger clusters. The polymer coating also protects the Fe_2O_3 core during the electrochemical reactions at high current densities. For the Fe_2O_3@rGO composite, the two components are combined in a different way: the Fe_2O_3 nanoparticles were directly grown on the rGO nanosheets and formed a 'rice-on-sheet' structure similar to what was reported [26]. The size and uniformity of the as-obtained Fe_2O_3 nanoparticles are comparable with those prepared without GO nanosheets, but the morphology is slightly different. Fe_2O_3@rGO nanoparticles are more oval, as shown in Fig. 2C and D, and embedded in the rGO sheets incompletely, with the part of the particles exposed, which may facilitate the fast kinetics in both important parts of the electrochemical reaction: lithium ion transport and electron conductivity. From TGA analysis shown in Fig. S2, the final amount of rGO and PEDOT:PSS is determined to be around 21% and 15%, respectively.

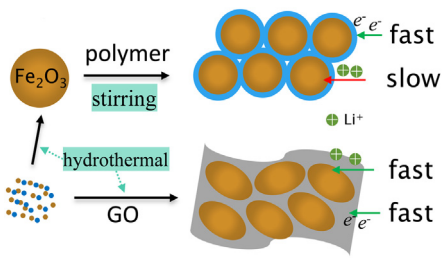

Scheme 1. Two routes to composites of Fe_2O_3 nanoparticles with conductive additives: *ex situ* coating of hydrothermally prepared Fe_2O_3@Polymer and *in situ* hydrothermal formation of Fe_2O_3@rGO.

The cyclic voltammetry (CV) study of bare Fe_2O_3 and Fe_2O_3 composites can help in understanding the mechanism of the electrochemical reactions at the electrode. Fig. 3 shows the CV scans in the potential range of 0.05–3 V (vs. Li^+/Li) at a scan rate of 0.2 mV s^{-1}. In good agreement with the previous reports, one pair of strong redox current peaks with separation over 1 V can be clearly seen. The difference in the first and second cathodic curves may be attributed to irreversible phase transformation during lithium insertion and extraction in the initial cycle [27]. The oxidation peak near 1.5–2.0 V in the anodic sweep (Fig. 3A) can be attributed to the formation of Fe^{3+} from Fe^0 [28]. The position of this oxidation peak for the three samples is fairly consistent during the cycling but demonstrates changes that are distinct for each type. It has been proposed that lithium storage in Fe_2O_3 proceeds *via* multiple steps, where lithiation involves transitions between the hexagonal $Li_xFe_2O_3$, cubic $Li_2Fe_2O_3$ and Fe(0) states summarized as the following reactions: [27,29,30]

$$Fe_2O_3 + xLi^+ + xe^- \rightarrow Li_xFe_2O_3$$

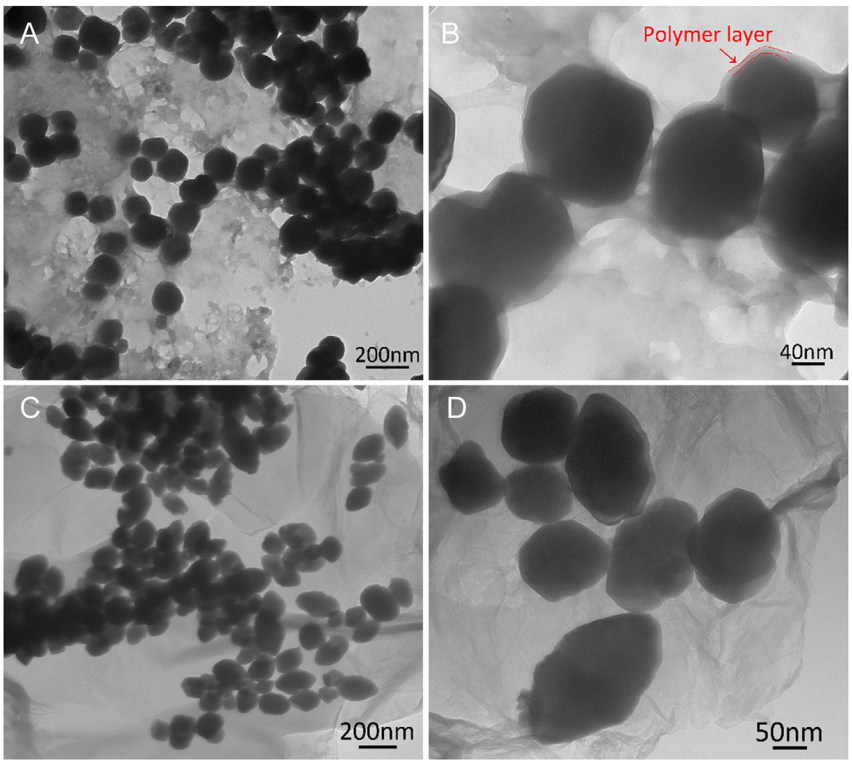

Fig. 2. (A) Low- and (B) high- magnification TEM images of Fe_2O_3@Polymer; (C) low- and (D) high-magnification TEM images of Fe_2O_3@rGO composites.

$$Li_xFe_2O_3 + (2-x)Li^+ + (2-x)e^- \rightarrow Li_2Fe_2O_3$$

$$Li_2Fe_2O_3 + 4Li^+ + 4e^- \rightarrow 2Fe + 3Li_2O$$

$$Fe_2O_3 + 6Li^+ + 6e^- \leftrightarrow 3Li_2O + 2Fe^0$$

The anodic peak intensity of bare Fe_2O_3 decreases from the second cycle, indicating some irreversible deterioration. At the same time, the cathodic peak shifts to a slightly lower potential without change in the current amplitude. The Fe_2O_3@Polymer composite demonstrates lower current intensities in both the anodic and cathodic sweeps. In addition, the cathodic peak shifts to a lower potential while the anodic peak shifts to a higher potential, resulting in a larger redox couple voltage window. On the other hand, from the CV study of Fe_2O_3@Polymer obtained at lower scanning rate of 0.1 mV s^{-1} shown in Fig. S3, the displacement of peaks is not as obvious as that obtained at higher scanning rate. We proposed that the greater hysteresis in voltage for Fe_2O_3@Polymer at higher scanning rate may be attributed to both electronic conductivity and the slower Li^+ diffusion caused by the 'blocking effect' of polymer which produces additional barrier that hinders the Li^+ transport for the initial cycles. As displayed in Scheme 1, Fe_2O_3 nanoparticles are fully covered with the polymer layer, which apparently hinders effective insertion of Li^+. The 3rd sweeping cycle is relatively similar to that of the bare Fe_2O_3, indicating the virtual completion of insertion of Li^+. rGO nanosheets in Fe_2O_3@rGO does not have such limitation because it has better exposure to the electrolyte. As a result, the Fe_2O_3@rGO ensures both fast Li^+ and electron kinetic transport, which leads to a fast electrochemical response. The CV curve of Fe_2O_3@rGO demonstrates the highest current intensities for the initial three cycles and its cathodic peak shifts to a higher potential coinciding with that in bare Fe_2O_3. The cathodic peak for the 3rd sweep was centered at about 0.75 V, which is higher than those of bare Fe_2O_3 and Fe_2O_3@Polymer, also indicating a quicker electrochemical response than the other two anodes.

Identical coin cells with metallic Li counter electrodes were used to evaluate the electrochemical performance of the Fe_2O_3 and the Fe_2O_3 composites. Fig. 4 shows the initial three galvanostatic charge–discharge cycles between 0.01 and 3 V vs. Li^+/Li at a current density of 50 mA g^{-1}. Large specific discharge capacities of about 1085, 1033, and 1186 mA h g^{-1} for the bare Fe_2O_3, Fe_2O_3@Polymer,

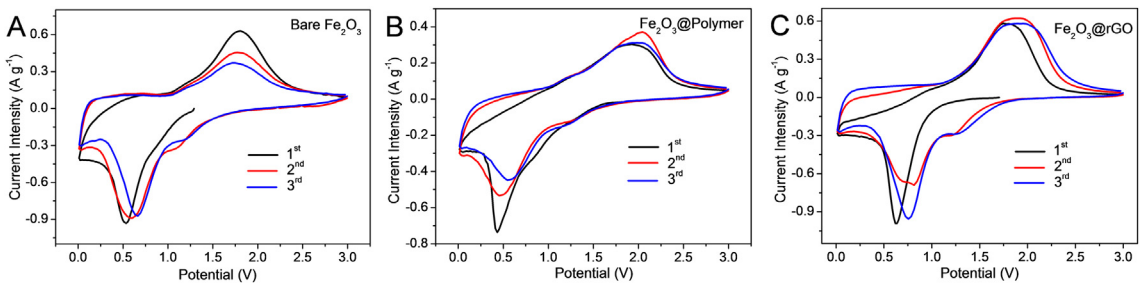

Fig. 3. Cyclic voltammetry (CV) curves of (A) bare Fe_2O_3; (B) Fe_2O_3@Polymer and (C) Fe_2O_3@rGO, respectively.

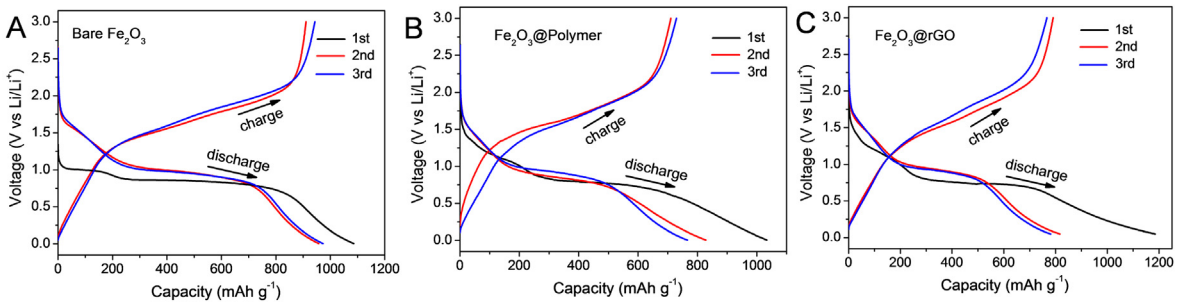

Fig. 4. Discharge and charge profile for the initial 3 cycles of (A) bare Fe_2O_3, (B) Fe_2O_3@Polymer and (C) Fe_2O_3@rGO electrodes cycled in the voltage range of 0.01–3.00 V vs. Li^+/Li.

and Fe_2O_3@rGO were achieved, and the reversible capacities were 910, 710, and 791 mA h g^{-1}, respectively. Although the addition of conductive agent could benefit the electrochemical performance by means of decreasing the overall resistance of coin cells, the amount of additives would necessarily lead to a decrease in theoretical capacity because they don't contribute to or lower the lithium storage capacity. We proposed that the reversible capacities were lower than the theoretical capacity of Fe_2O_3 may be due to the introduction of additives based on the TGA study (Fig. S2). Meanwhile, the reversible capacities calculated based on Fe_2O_3 only were 910, 899, and 930 mA h g^{-1} for the bare Fe_2O_3, Fe_2O_3@Polymer, and Fe_2O_3@rGO, respectively. Reversible capacity maintained around 90% of its theoretical capacity, indicating that Fe_2O_3 particles are electrochemically active. Obvious irreversible portions of the capacities during the first discharge–charge process are 175, 323, and 395 mA h g^{-1}, respectively. This trend may be attributed to the formation of the SEI layer at the electrode–electrolyte interface. Fe_2O_3@rGO experiences the largest capacity loss between the initial two cycles but then leads to the most stable cycling performance, indicating that SEI layer forms quickly. As shown in Fig. 5A, bare Fe_2O_3 delivers the highest initial capacity among the three but it fades precipitously upon further cycling. We speculate that the SEI layer formed during Li^+ insertion is unstable and decomposes catalyzed by the iron metal formed during the reduction process. Requirement for repeated formation/decomposition of the SEI layer leads to fast capacity fading [15].

Fe_2O_3@Polymer has the lowest initial capacity, apparently due to the polymer coating barrier hindering Li^+ transport. However, its stability exceeds that of the bare Fe_2O_3 because the SEI layer is more stable in the presence of the conductive polymer. Fe_2O_3@rGO demonstrates the best cycling performance due to advantages of rGO nanosheets wrapping and the capacity is about 527 mA h g^{-1} after 50 cycles, much higher than 401 and 350 mA h g^{-1} for Fe_2O_3@Polymer and bare Fe_2O_3, respectively. The Coulombic efficiency of the three electrodes maintains near 97% except for the first three cycles. Rate performances of the three samples are presented in Fig. 5B. Fe_2O_3@rGO delivers the discharge capacities of 746, 690 598, and 390 mA h g^{-1} at current densities of 100, 200, 400, and 800 mA g^{-1}, respectively. When the current density was reset to 50 mA g^{-1}, the discharge capacity rebounded to 736 mA h g^{-1}, which is ~98% of its initial value, indicating the excellent tolerance against the high current density of Fe_2O_3@rGO anode materials. For comparison, the capacity of bare Fe_2O_3 decreased more dramatically to 161 mA h g^{-1} at 800 mA g^{-1}. The performance of bare Fe_2O_3 was also not stable and had a large hysteresis as a function of the current densities – resetting the current density back to 50 mA g^{-1}, after high current density, not only did not recover to the original capacity but the value was rapidly declining. The Fe_2O_3@Polymer composite demonstrated a better stability than the bare Fe_2O_3. The capacity decrease with cycles was less pronounced at high current densities >200 mA g^{-1}. The dependence on the current density was also less dramatic – the capacity decreases from 355 to 306 mA g^{-1} when the current density increased from 400 to 800 mA g^{-1}. The presence of the gel-like polymer layer may provide a mild environment during the fast electrochemical reaction.

Electrochemical impedance spectrum (EIS) provides further information on the kinetics of electrochemical reactions at the electrode. The measurement was done with pristine cell for each sample (initial voltages are around 2.9–3.0 V). The Nyquist plots for the three electrodes were shown in Fig. 6. The semicircle observed in the high frequency range may be attributed to SEI formation and charge transfer resistance, indicating that the introduction of conductive additives can decrease the overall resistance and improve the conductivity. The following line of each electrode (Warburg line) in the low frequency region can be attributed to ion diffusion components [31]. The smaller electrochemical resistance for Fe_2O_3@rGO indicates a better conductivity of this composite.

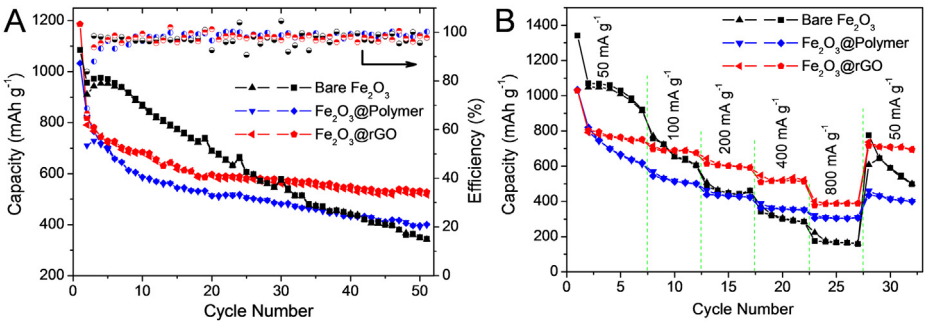

Fig. 5. (A) Cycling performance of the three types of anodes at a current density of 50 mA g^{-1} and their Coulombic efficiencies; (B) the rate performance of the three samples at different current densities.

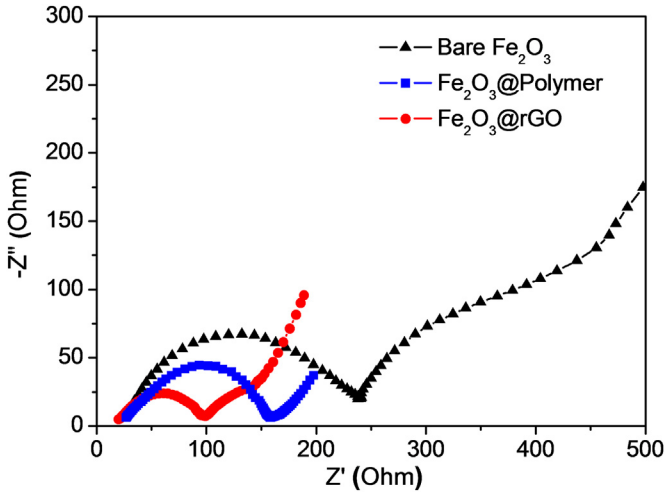

Fig. 6. Electrochemical impedance spectrum (EIS) of the three anode materials.

The overall behavior of three materials declines in the order Fe_2O_3@rGO > Fe_2O_3@Polymer > bare Fe_2O_3 and once again confirms that introduction of conductive additives can improve the electrochemical performance of anodes for lithium ion batteries.

4. Conclusion

In summary, different forms of lithium ion battery anode based on Fe_2O_3 nanoparticles prepared by a facile hydrothermal route were investigated including rGO nanosheets wrapped Fe_2O_3@rGO, conductive polymer (PEDOT:PSS) coated Fe_2O_3@Polymer, as well as bare Fe_2O_3. The addition of conductive polymer layer in Fe_2O_3@-Polymer facilitates the electron transport but may hinder the Li^+ ion insertion at higher current density. On the other hand, Fe_2O_3@rGO prepared by growing Fe_2O_3 nanoparticles directly on rGO shows the best electrochemical behavior due to a beneficial combination of the rGO nanosheets partially wrapped around Fe_2O_3 which facilitate both the electron transport and Li^+ ion insertion. Its superior cycling and rate performance demonstrates faster and more stable SEI layer formation. The high specific capacity and stable rate performance of Fe_2O_3@rGO composites encourage their further study to be potential candidate for the anode materials in LIBs. These results will be helpful in further elucidation of the role of conductive additives in improving the electrochemical performance of Fe_2O_3 based composite anodes.

Acknowledgments

We acknowledge the funding support from NSF/CMMI Nano-Manufacturing Program under Grant No. 1131290 and the office of Vice President for Research at NMSU. L. F. acknowledges the Preparing Future Faculty Graduate Assistantship Award. R. R. is supported by NSF New Mexico Alliance for Minority Participation (AMP) Program under Grant No: HRD-135011.

Appendix A. Supplementary data

Supplementary data related to this article can be found at http://dx.doi.org/10.1016/j.jpowsour.2014.02.096.

References

[1] S. Chu, A. Majumdar, Nature 488 (2012) 294–303.
[2] J.B. Goodenough, Y. Kim, Chem. Mater. 22 (2010) 587–603.
[3] J.B. Goodenough, K.-S. Park, J. Am. Chem. Soc. 135 (2013) 1167–1176.
[4] Q. Su, D. Xie, J. Zhang, G. Du, B. Xu, ACS Nano. 7 (2013) 9115–9121.
[5] C. Xu, Y. Zeng, X. Rui, J. Zhu, H. Tan, A. Guerrero, J. Toribio, J. Bisquert, G. Garcia-Belmonte, Q. Yan, J. Phys. Chem. C. 117 (2013) 17462–17469.
[6] J.X. Zhu, Z.Y. Yin, D. Yang, T. Sun, H. Yu, H.E. Hoster, H.H. Hng, H. Zhang, Q.Y. Yan, Energ. Environ. Sci. 6 (2013) 987–993.
[7] L. Ji, Z. Lin, M. Alcoutlabi, X. Zhang, Energ. Environ. Sci. 4 (2011) 2682–2699.
[8] J.J. Zhang, Y.F. Sun, Y. Yao, T. Huang, A.S. Yu, J. Power Sources 222 (2013) 59–65.
[9] B. Wang, J.S. Chen, H.B. Wu, Z. Wang, X.W. Lou, J. Am. Chem. Soc. 133 (2011) 17146–17148.
[10] Y.-M. Lin, P.R. Abel, A. Heller, C.B. Mullins, J. Phys. Chem. Lett. 2 (2011) 2885–2891.
[11] X. Xu, R. Cao, S. Jeong, J. Cho, Nano Lett. 12 (2012) 4988–4991.
[12] Z. Wang, D. Luan, S. Madhavi, C. Ming Li, X. Wen Lou, Chem. Commun. 47 (2011) 8061–8063.
[13] L. Zhang, H.B. Wu, S. Madhavi, H.H. Hng, X.W. Lou, J. Am. Chem. Soc. 134 (2012) 17388–17391.
[14] L. Ji, O. Toprakci, M. Alcoutlabi, Y. Yao, Y. Li, S. Zhang, B. Guo, Z. Lin, X. Zhang, ACS Appl. Mater. Interfaces 4 (2012) 2672–2679.
[15] F. Han, D. Li, W.C. Li, C. Lei, Q. Sun, A.H. Lu, Adv. Funct. Mater. 23 (2013) 1692–1700.
[16] J.-M. Jeong, B.G. Choi, S.C. Lee, K.G. Lee, S.-J. Chang, Y.-K. Han, Y.B. Lee, H.U. Lee, S. Kwon, G. Lee, C.-S. Lee, Y.S. Huh, Adv. Mater. 25 (2013) 6250–6255.
[17] Y. Ma, G. Ji, J.Y. Lee, J. Mater. Chem. 21 (2011) 13009–13014.
[18] W. Qin, C. Yang, R. Yi, G. Gao, J. Nanomater. 2011 (2011), http://dx.doi.org/10.1155/2011/159259.
[19] Y. Xu, R. Yi, B. Yuan, X. Wu, M. Dunwell, Q. Lin, L. Fei, S. Deng, P. Andersen, D. Wang, H. Luo, J. Phys. Chem. Lett. 3 (2012) 309–314.
[20] M.S.A. Sher Shah, A.R. Park, K. Zhang, J.H. Park, P.J. Yoo, ACS Appl. Mater. Interfaces 4 (2012) 3893–3901.
[21] G.K. Pradhan, D.K. Padhi, K.M. Parida, ACS Appl. Mater. Interfaces 5 (2013) 9101–9110.
[22] Y. Yao, Z. Yang, H. Sun, S. Wang, Ind. Eng. Chem. Res. 51 (2012) 14958–14965.
[23] Z. Li, F. Gong, G. Zhou, Z.-S. Wang, J. Phys. Chem. C. 117 (2013) 6561–6566.
[24] L. Fei, Q. Lin, B. Yuan, G. Chen, P. Xie, Y. Li, Y. Xu, S. Deng, S. Smirnov, H. Luo, ACS Appl. Mater. Interfaces 5 (2013) 5330–5335.
[25] X. Zhu, Y. Zhu, S. Murali, M.D. Stoller, R.S. Ruoff, ACS Nano 5 (2011) 3333–3338.
[26] Y. Zou, J. Kan, Y. Wang, J. Phys. Chem. C. 115 (2011) 20747–20753.
[27] S. Chaudhari, M. Srinivasan, J. Mater. Chem. 22 (2012) 23049–23056.
[28] J. Morales, L. Sánchez, F. Martín, F. Berry, X. Ren, J. Electrochem. Soc. 152 (2005) A1748–A1754.
[29] H. Xiao, Y. Xia, W.K. Zhang, H. Huang, Y.P. Gan, X.Y. Tao, J. Mater. Chem. A 1 (2013) 2307–2312.
[30] D. Larcher, C. Masquelier, D. Bonnin, Y. Chabre, V. Masson, J.-B. Leriche, J.-M. Tarascon, J. Electrochem. Soc. 150 (2003) A133–A139.
[31] M. Zhang, B. Qu, D. Lei, Y. Chen, X. Yu, L. Chen, Q. Li, Y. Wang, T. Wang, J. Mater. Chem. 22 (2012) 3868–3874.